Electronic Supplementary Information

DNA Photocleavage in Anaerobic Conditions by a Ru(II) Complex: a New Mechanism

Yue Zheng,[a,b] Qianxiong Zhou,*[a] Wanhua Lei,[a] Yuanjun Hou,[a] Ke Li,[a,b] Yongjie Chen,[a,b] Baowen Zhang,[a] Xuesong Wang*[a]

[a]*Key Laboratory of Photochemical Conversion and Optoelectronic Materials, Technical Institute of Physics and Chemistry,*
Chinese Academy of Sciences, Beijing 100190, P. R. China. Fax: +86-10-62564049; Tel: +86-10-82543592; E-mail:xswang@mail.ipc.ac.cn (X.Wang); zhouqianxiong@mail.ipc.ac.cn (Q. Zhou).
[b]*Graduate School of Chinese Academy of Sciences, Beijing 100049, P. R. China.*

Experimental Section

Materials. $RuCl_3.3H_2O$, 2,2'-bipyridine, 2-pyridinesulfonic acid, DMPO (5,5-dimethyl-1-pyrroline-*N*-oxide), TEMPO (2,2,6,6-tetrametyl piperidine-1-oxyl), gel loading buffer and tris-hydroxymethyl-aminomethane (Tris base) were purchased from Sigma Aldrich. The supercoiled pBR322 plasmid DNA was obtained from TaKaRa Biotechology Company. $Ru(bpy)_2Cl_2$ was synthesized by the reported methods.[1]

Instruments and methods. ^1H and ^{13}C NMR spectra were obtained on a Bruker DMX-400 MHz and 100 MHz spectrophotometer. High-resolution ESI mass spectrometry (HR ESI-MS) spectra were determined on a Brucker APEX IV (7.0T) FT_MS. UV-vis absorption spectra were recorded on a Shimadzu UV-1601 spectrophotometer. Elemental analysis was performed on an Elementar Vario EL instrument.

The EPR spectra were measured on a Bruker ESP-300E spectrometer at 9.8 GHz, X-band, with 100 Hz field modulation. Samples were injected quantitatively into quartz capillaries, purged with argon for 20 min in the dark, and illuminated in the cavity of the EPR spectrometer with a Nd:YAG laser at 355 nm (5-6 ns of pulse width, 10 Hz of repetition frequency, 30 mJ/pulse energy).

The electrochemical properties were measured on an EG&G Model283 Potentiostat/Galvanostat in a three-electrode cell with a glassy carbon working electrode, a Pt counter electrode, and a saturated calomel electrode (SCE) as reference. The cyclic voltammetry was conducted at a scan rate of 50 mV s^{-1} in Ar-saturated, anhydrous CH_3CN containing 0.1 M tetra-*n*-butylammonium hexafluorophosphate as the supporting electrolyte.

Singlet oxygen was detected by monitoring its NIR emission at around 1270 nm on an Edinburgh Analytical Instruments (FLSP 920) spectrofluorimeter equipped with a NIR-PMT detector (R5509, Hamamatsu) cooled to -80°C.

The photoinduced ligand dissociation experiments were carried out under irradiation of a 500 W high pressure sodium lamp, using a long pass glass filter to cut off the wavelengths shorter than 470 nm.

Supercoiled pBR322 plasmid DNA was used to study DNA photodamage. 40 μL of pBR322 plasmid DNA (40 μg/mL) was incubated with a complex dosed from 0 to 50 μM. The mixture was irradiated with visible light (≥ 470 nm) for 15 minutes by a 500 W high pressure sodium lamp. After irradiation and incubation at room temperature for 2 h, 10 μL Loading buffer was added. 10 μL of sample was taken for agarose gel (1%) electrophoresis (in Tris-acetic acid-EDTA buffer, pH 8.0) at 5 V/cm for 1.5 h. The gel was stained with EB (1 mg/L in H_2O) for 0.5 h and then analyzed using a Gel Doc XR system (Bio-Rad).

Anaerobic conditions were obtained by bubbling the solutions with high-purity argon for 20 min. All measurements were carried out at room temperature.

Cell survival assay: Human pulmonary adenocarcinoma A549 cells were cultured in DMEM medium supplemented with glutamax, 10% serum supreme and 1% penicillin/streptomycin at 37°C under atmosphere containing 5% CO_2. A549 Cells were plated in DMEM medium in ViewPlate 96 well plates at 3000 cells/well and incubated for 24 h. The complex was dosed from 0 to 100 µM, incubated with the cells for 12 h, and then irradiated for 30 min with a 15 W LED lamp (λ = 470 nm). The cells were then incubated for 48 h followed by the addition of Cell Titer Glo (Promega) to determine viability.[2] Dark controls were run in parallel. The resulting luminescence was measured on a Multimode Plate Reader (EnSpire). Data were analysed using reported procedures.[2]

Synthesis of $[Ru(bpy)_2(py\text{-}SO_3)](PF_6)$. To a solution containing 35 mg (0.22 mmol) of 2-pyridinesulfonic acid in 5 mL of 10:1 methanol/water, 12 mg (0.22 mmol) of KOH was added. The mixture was stirred for 0.5 h, followed by adding 100 mg (0.2 mmol) $Ru(bpy)_2Cl_2$ and then refluxed for 2 h under N_2 atmosphere. After removal of the solvent, the solid was purified on silica gel using $CH_3CN/H_2O/KNO_3$ (100:4:1) as eluent. The compound was dissolved in water and precipitated with NH_4PF_6. The red solid was filtered, washed with water and vacuum dried. Yield 68%.^{1}H NMR (400 MHz, d_6-acetone) δ 9.26(d, *J* = 5.1 Hz, 1H), 8.67-8.80(m, 4H), 8.45(d, *J* = 5.2 Hz, 1H), 8.28-8.19(m, 2H), 8.14-7.98(m, 4H), 7.95-7.84(m, 2H), 7.82(d, *J* = 5.1 Hz, 1H), 7.70-7.63(m, 1H), 7.56(d, *J* = 5.3 Hz, 1H), 7.47-7.35(m, 3H). ^{13}C NMR (100 MHz, CD_3CN): δ (ppm) 156.02, 155.59, 154.16, 153.47, 152.89, 149.75, 148.76, 148.19, 146.63, 146.60, 134.74, 133.39, 133.31, 133.11, 132.09, 123.94, 123.00, 122.59, 122.53, 122.23, 120.03, 119.97, 119.64, 119.30, 119.18 (Figure S23). HR ESI-MS: m/z = 572.0316 for $(M\text{-}PF_6)^+$ (Figure S22)**.** Anal. Calcd for $C_{25}H_{20}F_6N_5O_3PRuS\cdot 2.5H_2O$: C, 39.37; H, 3.30; N, 9.19. Found: C, 39.30; H, 3.34; N, 9.26.

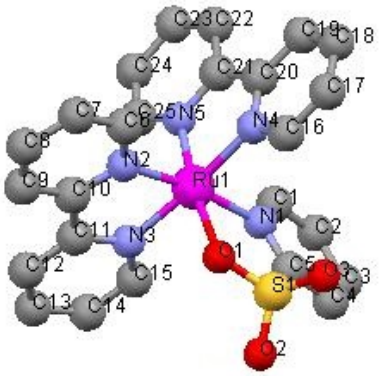

Figure S1. Crystal structure of $[Ru(bpy)_2(py\text{-}SO_3)](PF_6)$ with thermal ellipsoids at 50% probability (PF_6^-, CH_3CN and hydrogen atoms are omitted for clarity).

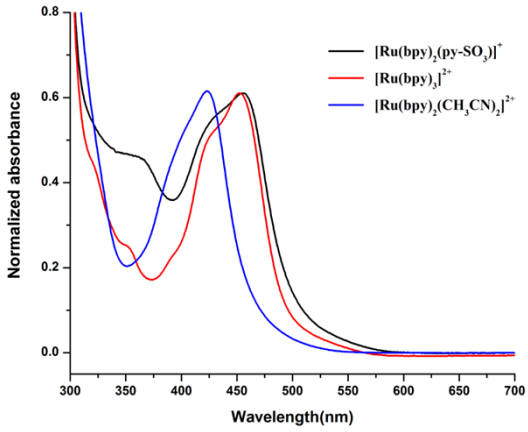

Figure S2. Normalized absorption spectra of the examined Ru(II) complexes in aqueous solutions.

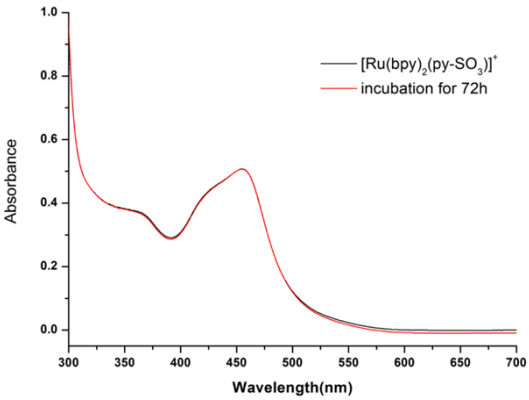

Figure S3. Absorption spectra of $[Ru(bpy)_2(py\text{-}SO_3)]^+$(50μM) in aqueous solutions freshly prepared and after standing for 72 h in the dark.

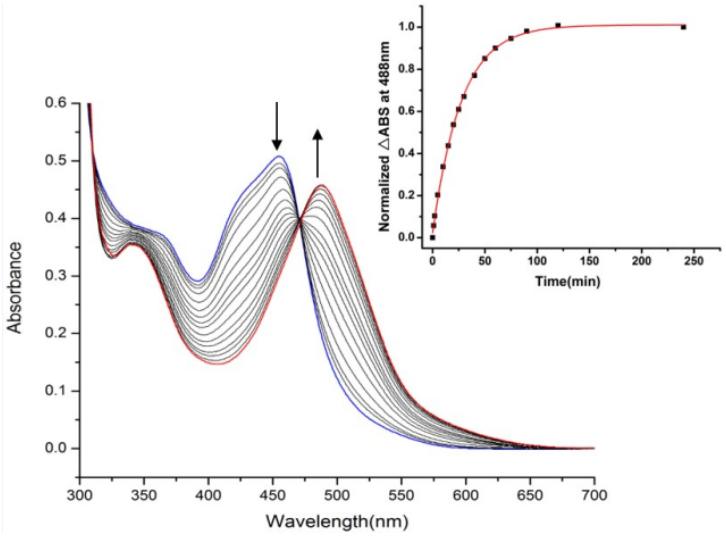

Figure S4. Absorption spectrum changes of $[Ru(bpy)_2(py\text{-}SO_3)]^+$ (50 μM) in aqueous solution upon irradiation (≥ 470 nm). Inset shows the normalized absorbance changes at 488 nm as a function of irradiation time.

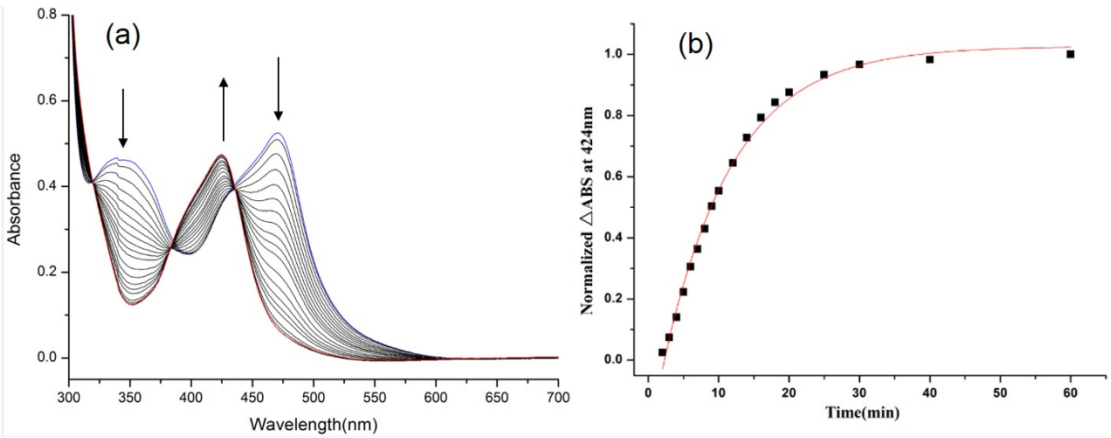

Figure S5. (a) Absorption spectra changes of $[Ru(bpy)_2(py\text{-}SO_3)]^+$ (50 μM) in Ar-saturated CH_3CN upon irradiation (≥ 470 nm), (b) absorbance changes at 424 nm as a function of irradiation time.

^{1}H NMR experiments provide more direct evidence for the dissociation of py-SO_3. In D_2O (Figure S6), irradiation led to two new resonant peaks at 9.68 and 9.39 ppm, assignable to mono-aqua and bis-aqua ligand-substitution products, respectively. Due to a much higher concentration of $[Ru(bpy)_2(py\text{-}SO_3)]^+$ (in mM level) was used in NMR than in UV-vis absorption measurements, the intermediate in which py-SO_3 binds on Ru center by only N atom (*i.e.* mono-aquated product) was detected. In CD_3CN (Figure S7), more efficient ligand dissociation allowed for full conversion of $[Ru(bpy)_2(py\text{-}SO_3)]^+$. Thus, the final ^{1}H NMR spectrum may be unambiguously attributed to $[Ru(bpy)_2(CH_3CN)_2]^{2+}$ and free py-SO_3.

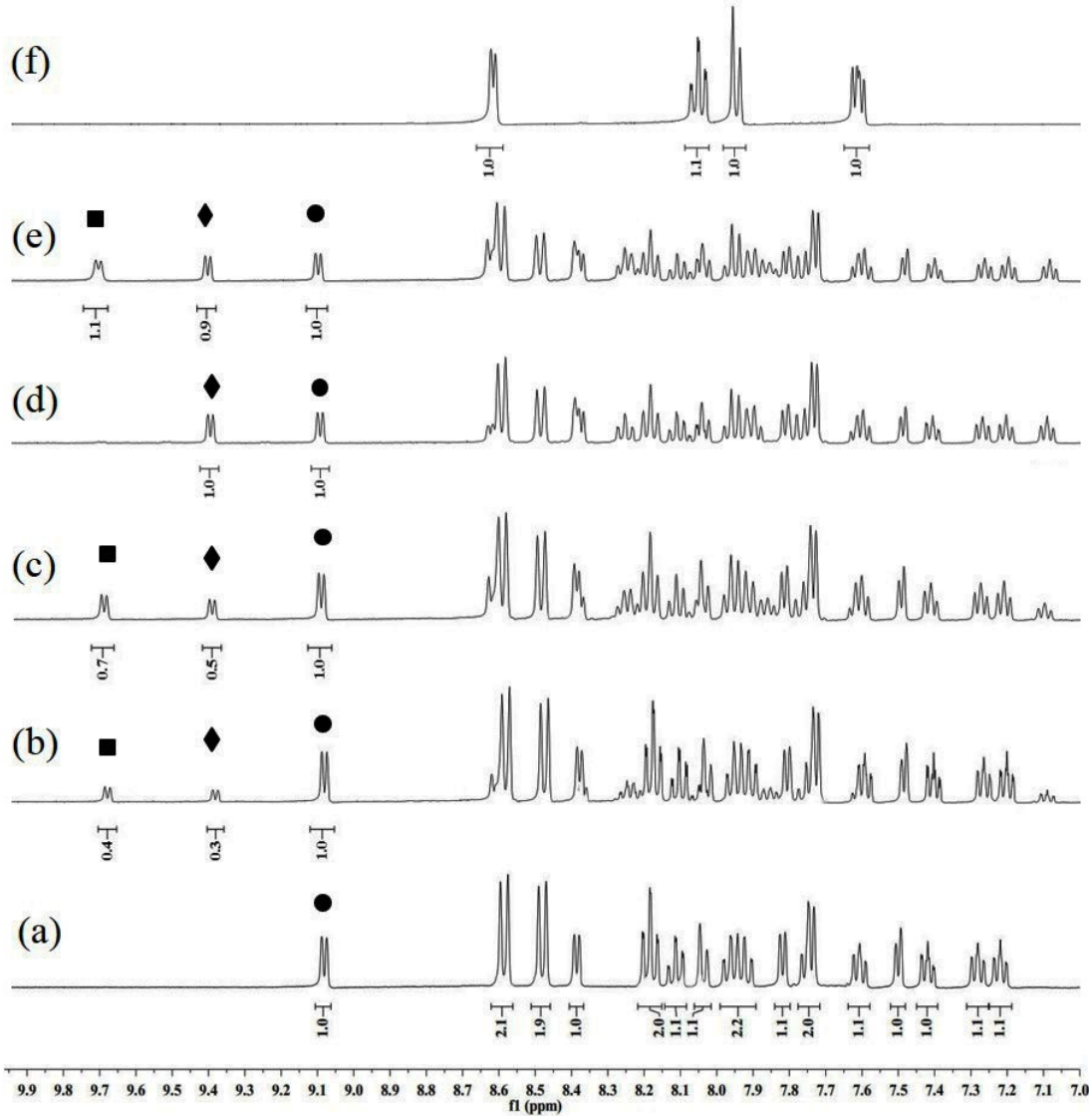

Figure S6. ^{1}H NMR spectra changes of $[Ru(bpy)_2(py\text{-}SO_3)]^+$ in Ar-saturated D_2O upon irradiation ($\lambda_{irr} \geq 470$ nm), (a) before irradiation, (b) irradiation for 30 min, (c) irradiation for 60 min, (d) irradiation for 60 min and then standing in the dark for 2 h, (e) irradiation for 120 min, (f) ^{1}H NMR spectrum of py-SO_3H in D_2O in the presence of NaOH.

The doublet at 9.08 ppm (labeled by●) may be attributed to the aromatic proton on C16 (see Figure S1). Due to its closest proximity to the py-SO_3 ligand, the sensitivity of its chemical shift to the photodissociation of py-SO_3 is expected. Upon irradiation, H(16) exhibited two new doublets at 9.39 ppm and 9.68 ppm, assignable to bis-aquated (labeled by ♦) and mono-aquated (labeled by ■) products, respectively. The assignment is based on the fact that the doublet at 9.68 ppm disappeared after standing of the irradiated sample in the dark for 2 h. The most reasonable explanation for this finding is that the mono-aquated product, in which py-SO_3 binds on Ru(II) center by only N atom, is just an intermediate and can transform to either $[Ru(bpy)_2(py\text{-}SO_3)]^+$or $[Ru(bpy)_2(D_2O)]^{2+}$. Additionally, The resonant signals of the released free py-SO_3 are discernible, particularly at 8.60 and 7.61 ppm, though overlap with the signals of $[Ru(bpy)_2(py\text{-}SO_3)]^+$ is obvious.

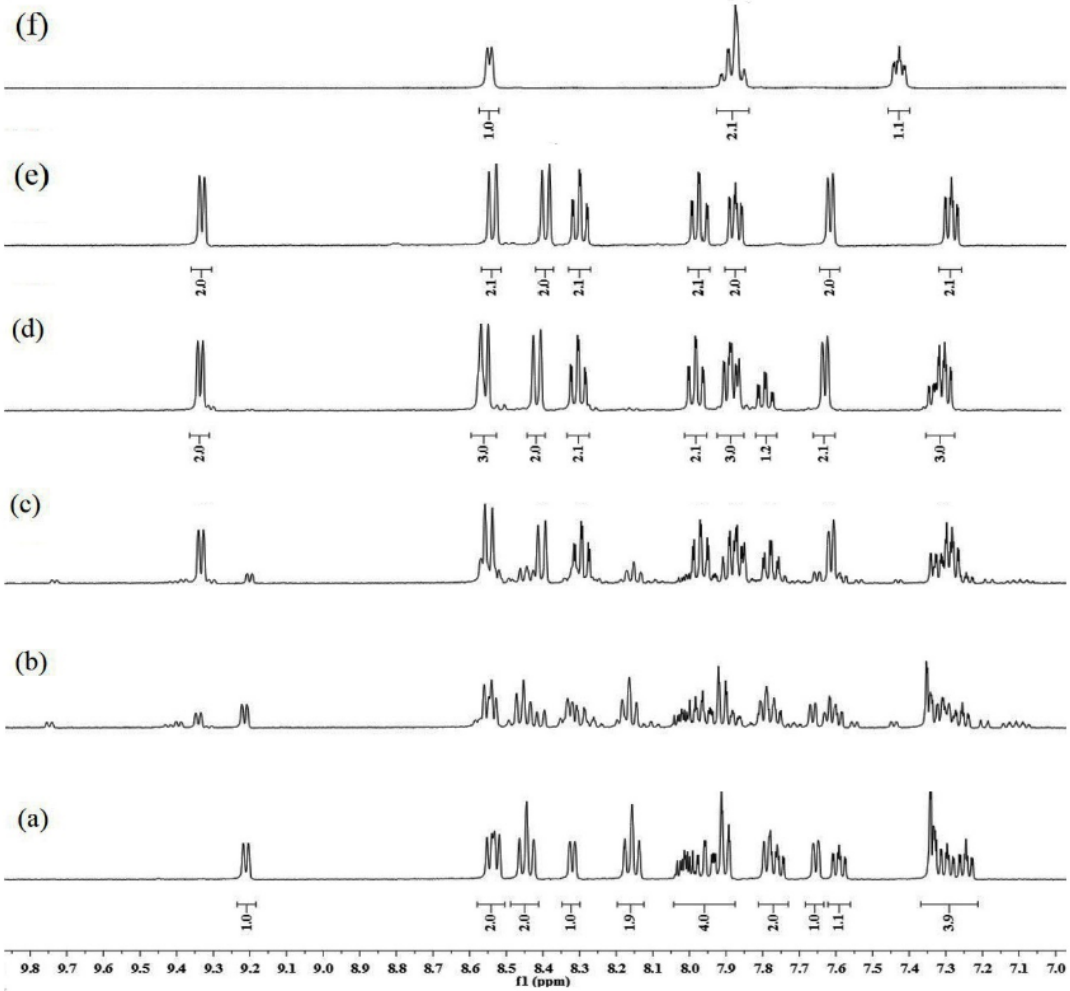

Figure S7. ^1H NMR spectra changes of $[Ru(bpy)_2(py\text{-}SO_3)]^+$ in Ar-saturated CD_3CN upon irradiation ($\lambda_{irr} \geq 470$ nm),(a)-(d) irradiation for 0 min, 15 min, 30 min, and 60min, respectively, (e) ^1H NMR spectrum of $[Ru(bpy)_2(CH_3CN)_2]^{2+}$ in CD_3CN, (f) ^1H NMR spectrum of py-SO_3H in

CD_3CN in the presence of NaOH.

It is clear that some resonant peaks of the released py-SO_3 experienced significant high field shifts (*e.g.* 7.42 ppm to *ca.*7.31ppm，7.87 ppm to *ca.*7.78 ppm) with respect to that of py-SO_3H in the presence of NaOH. This may be attributed to the ion pairing effect between the released py-SO_3 and the resultant Ru(II) product in the solvent (CD_3CN) of low dielectric constant. The ion pairing effect is negligible in D_2O, as shown in Figure S6.

High-resolution ESI-MS support the photodissociation of py-SO_3 further (Figure S8). Irradiation of $[Ru(bpy)_2(py\text{-}SO_3)]^+$ in CH_3COCH_3/H_2O mixed solvent in the presence of 9-ethylguanine (9-EtG) gave two m/z signals at 296.5610 and 592.1143 in the positive field, assignable to $[Ru(bpy)_2(9\text{-}EtG)]^{2+}$ and $[Ru(bpy)_2(9\text{-}EtG)\text{-}H]^+$, respectively. In the negative field, a m/z signal at 157.9915 was also observed, attributable to py-SO_3. These findings vindicate the photodissociation of py-SO_3 and demonstrate the coordination potential of the resultant Ru(II) fragment toward nucleobases.

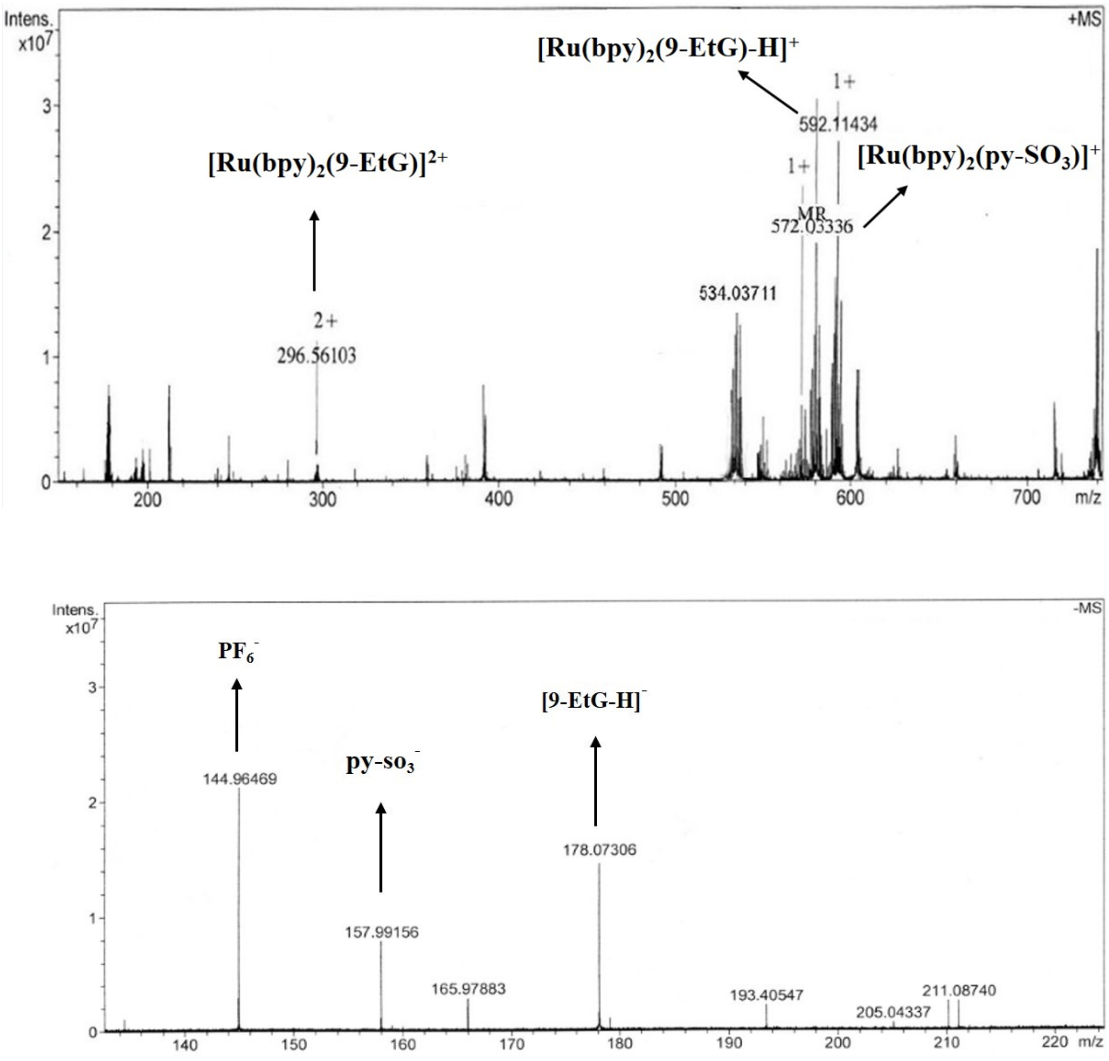

Figure S8. HR ESI-MS spectra of $[Ru(bpy)_2(py\text{-}SO_3)]^+$ in Ar-saturated CH_3COCH_3:H_2O (1.5:1 in volume ratio) after irradiation for 1 h in the presence of 9-EtG. The upper and bottom spectra were obtained in positive and negative field, respectively.

Irradiation of the Ar-saturated solution of $[Ru(bpy)_2(py\text{-}SO_3)]^+$ and 9-EtG led to two new resonant signals at 8.82 ppm and 6.96 ppm with respect to Figure S6. The former may be attributed to the aromatic proton on C16 of the Ru fragment that has been coordinated by 9-EtG. The later may be ascribed to the aromatic proton of 9-EtG that has coordinated onto Ru center. Upon coordination, the chemical shift of 9-EtG underwent a dramatic high field shift. Similar result was also observed in covalent binding of 9-EtG to a Ru arene complex.[3]

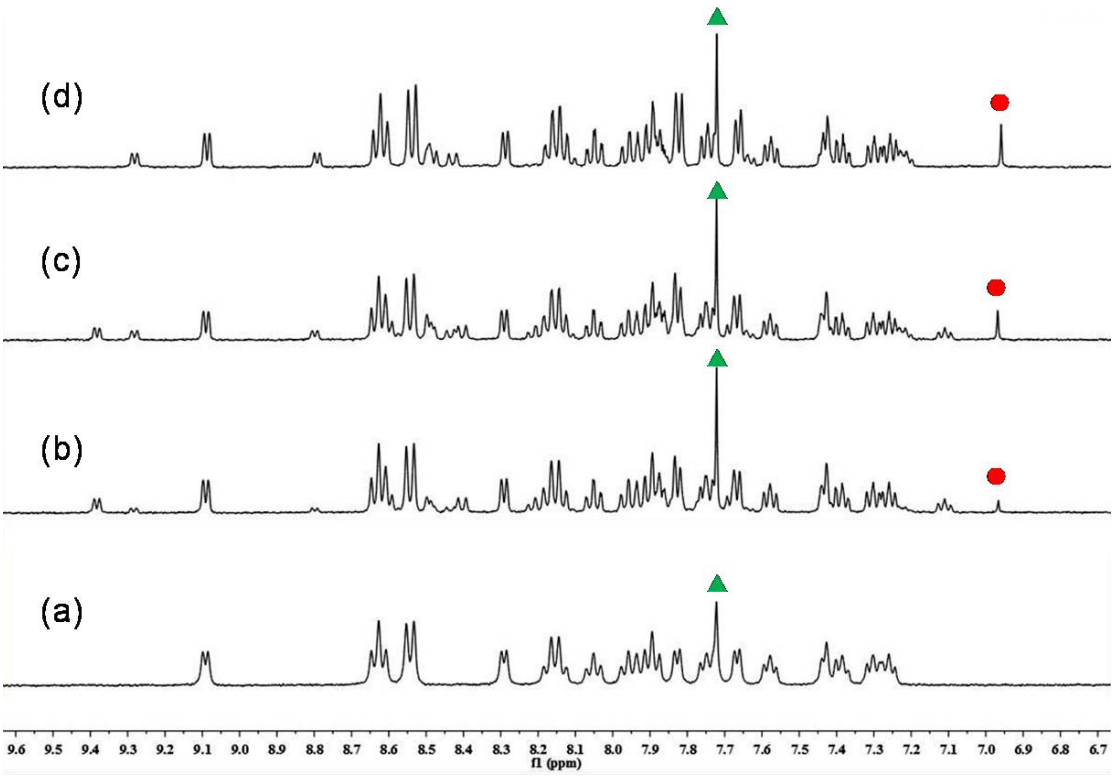

Figure S9. ^1H NMR spectra changes of $[Ru(bpy)_2(py\text{-}SO_3)]^+$ in Ar-saturated CD_3COCD_3/D_2O (1.5:1) upon irradiation ($\lambda_{irr} \geq 470$ nm) in the presence of excess 9-EtG. (a) before irradiation, (b) irradiation for 30 min, (c) irradiation for 60 min, (d) irradiation for 60 min and then standing in the dark for 12 h. ▲ and ● indicate the H8 of the free and bound 9-EtG, respectively.

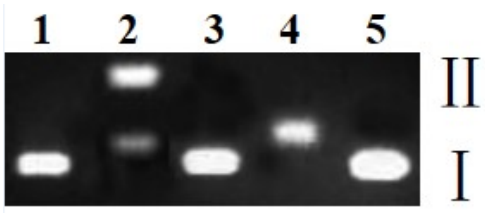

Figure S10. Agarose gel electrophoresis pattern of pBR322 DNA (100 μM in base pairs) in Ar-saturated Tris-EDTA (5 mM, pH = 7.5) upon irradiation (≥ 470 nm) for 15 min in different conditions. Lane 1: DNA alone; lane 2: DNA + $[Ru(bpy)_2(py\text{-}SO_3)]^+$ (10 μM); lane 3: DNA + $[Ru(bpy)_3]^{2+}$ (50 μM); lane 4: DNA + $[Ru(bpy)_2(CH_3CN)_2]^{2+}$ (20 μM); lane 5: DNA + 2-pyridinesulfonic acid (50 μM). Form I and form II denote supercoiled circular and nicked circular forms, respectively($\lambda_{irr} \geq 470$ nm).

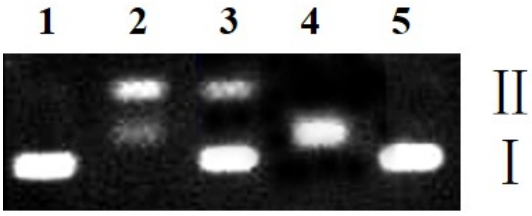

Figure S11. Agarose gel electrophoresis pattern of pBR322 DNA (100 μM in base pairs) in air-saturated Tris-EDTA (5 mM, pH = 7.5) upon irradiation (≥ 470 nm) for 15 min in different conditions. Lane1: DNA alone; lane 2: DNA + $[Ru(bpy)_2(py\text{-}SO_3)]^+$; lane 3: DNA + $[Ru(bpy)_3]^{2+}$; lane 4: DNA + $[Ru(bpy)_2(CH_3CN)_2]^{2+}$; lane 5: DNA + $[Ru(bpy)_2(py\text{-}SO_3)]^+$ (100 μM), dark control. Form I and form II denote supercoiled circular and nicked circular forms, respectively. [complex] = 20 μM.

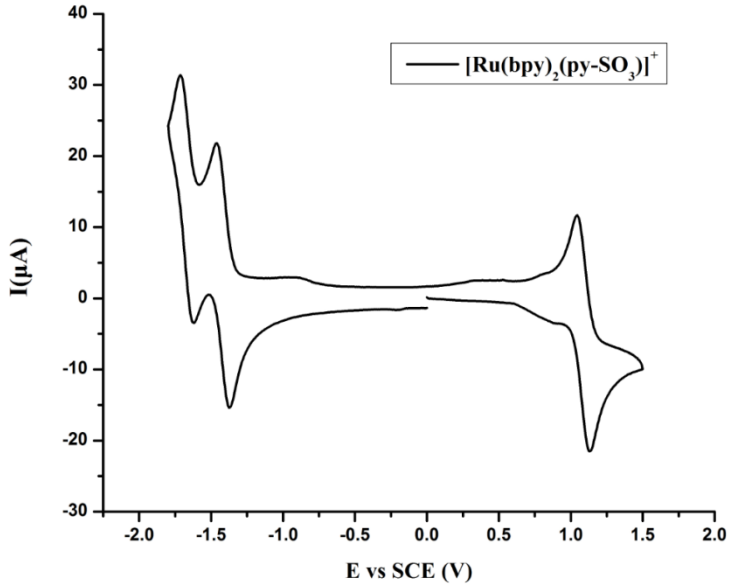

Figure S12. Cyclic voltammograms of $[Ru(bpy)_2(py\text{-}SO_3)]^+$ in Ar-saturated CH_3CN. Scan rate is 50 mV/s.

$[Ru(bpy)_2(py\text{-}SO_3)]^+$ showed one oxidation potential, attributable to Ru(III)/Ru(II) couple, at +1.08 V *vs* SCE in Ar-saturated CH_3CN, and two reduction waves at -1.42 V and -1.67 V, attributed to the sequential reduction of each bpy ligand. In contrast, $[Ru(bpy)_3]^{2+}$ exhibited redox potentials at +1.29 V, -1.33 V, -1.52 V and -1.76 V, respectively, in the same condition. Obviously, the oxidizing ability of $[Ru(bpy)_2(py\text{-}SO_3)]^+$ is lower than that of $[Ru(bpy)_3]^{2+}$ in either ground or excited state. It is well known that the ^{3}MLCT state of $[Ru(bpy)_3]^{2+}$ cannot lead to oxidative damage to DNA. Thus, the role of ^{3}MLCT may be excluded in the DNA photocleavage by $[Ru(bpy)_2(py\text{-}SO_3)]^+$ in hypoxic condition.

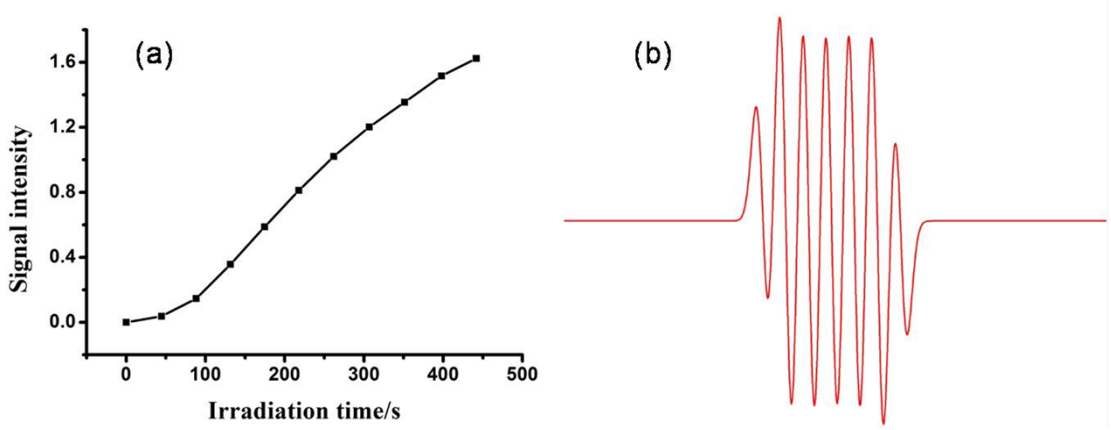

Figure S13. (a) EPR signal intensity as a function of irradiation time, which were obtained after laser irradiation (355 nm) of an Ar-saturated CH_3CN solution of $[Ru(bpy)_2(py\text{-}SO_3)]^+$ (1 mM) and DMPO (50 mM); (b) Simulated EPR spectrum using $a^N = 6.8$ G, $a_\gamma^{H1} = 3.5$ G and $a_\gamma^{H2} = 3.3$ G.

DMPOX may originate from the reaction of $^1O_2$ with DMPO.[4] Despite our EPR experiments were performed in Ar-saturated solutions, we still examined the possibility of this mechanism. By monitoring the phosphorescence of $^1O_2$ at ca.1270 nm,[5] we found that the $^1O_2$ generation ability of $[Ru(bpy)_2(py\text{-}SO_3)]^+$ is far lower than that of $[Ru(bpy)_3]^{2+}$. No discernible $^1O_2$ phosphorescence was detected even in O_2-saturated CH_3CN (Figure S13). On the other hand, we did not record DMPOX signal upon irradiation of $[Ru(bpy)_3]^{2+}$ in Ar-saturated CH_3CN (Figure S14). Thus, $^1O_2$ mechanism may be excluded definitely.

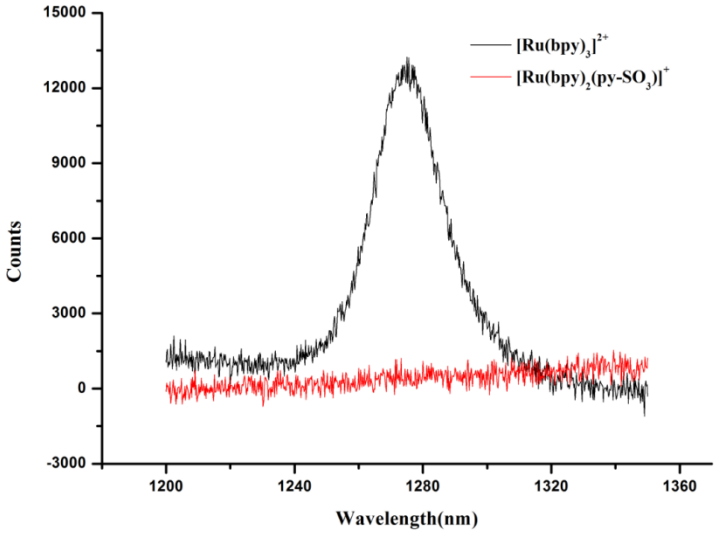

Figure S14. NIR emission spectra obtained upon laser irradiation (450 nm) of $[Ru(bpy)_2(py\text{-}SO_3)]^+$ (50μM, red curve) or $[Ru(bpy)_3]^{2+}$(50 μM, black curve) in O_2-saturated CH_3CN solution.

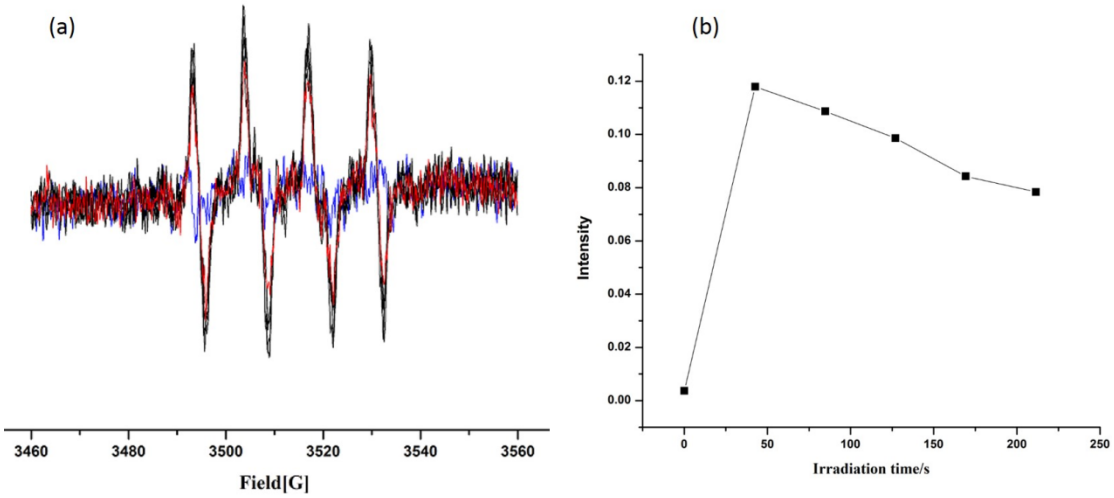

Figure S15. (a) EPR signals obtained upon laser irradiation (355 nm) of an Ar-saturated CH_3CN solution of $[Ru(bpy)_3]^{2+}$ (1 mM) and DMPO (50 mM). (b) EPR signal instensity changes as a function of irradiation time. The EPR signals obtained in this condition may be attributed to the adduct of DMPO and superoxide anion radical ($O_2^{\cdot-}$). The residue O_2 is responsible for the formation of $O_2^{\cdot-}$. With the gradual consumption of O_2, the signal intensity decreased gradually.

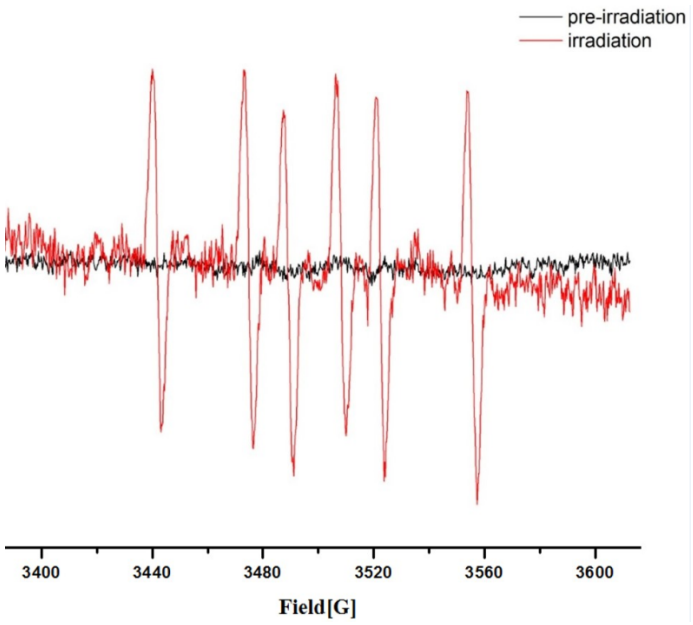

Figure S16. EPR spectrum obtained upon laser irradiation (355 nm) of an Ar-saturated DMSO solution of $[Ru(bpy)_2(py\text{-}SO_3)]^{+}$(1 mM) and DMPO (50 mM).

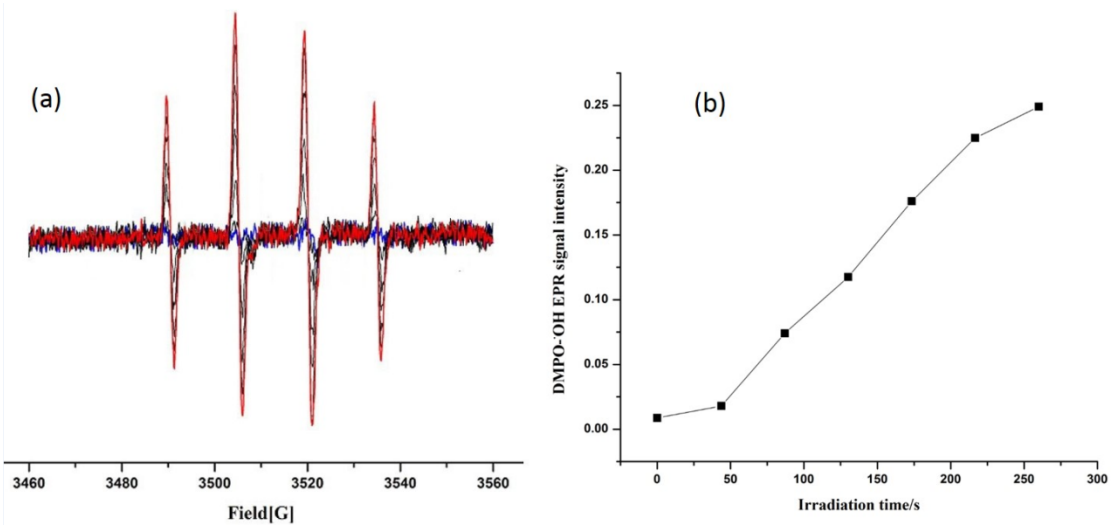

Figure S17. (a) EPR signals obtained upon laser irradiation (355 nm) of an Ar-saturated aqueous solution of $[Ru(bpy)_2(py\text{-}SO_3)]^+$ (1 mM) and DMPO (50 mM). (b) EPR signal intensity changes as a function of irradiation time.

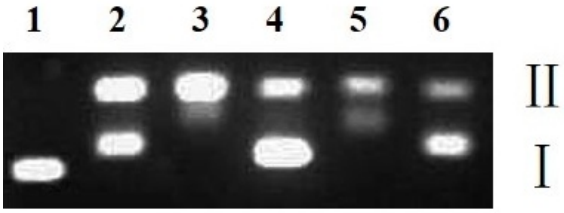

Figure S18. Agarose gel (1%) electrophoresis pattern of pBR322 DNA (100 μM in base pairs) in Ar-saturated Tris-EDTA (5 mM, pH = 7.5) upon irradiation (≥ 470 nm) for 15 min in different conditions. Lane 1: DNA alone; lane 2: DNA + $[Ru(bpy)_2(py\text{-}SO_3)]^+$ (10 μM); lane 3: DNA + $[Ru(bpy)_2(py\text{-}SO_3)]^+$ (20 μM); lane 4: DNA + $[Ru(bpy)_2(py\text{-}SO_3)]^+$ (20 μM) + DMSO (0.28 M); lane 5: DNA + $[Ru(bpy)_2(py\text{-}SO_3)]^+$ (20 μM) + TEMPO (10 mM); lane 6: DNA + $[Ru(bpy)_2(py\text{-}SO_3)]^+$ (20 μM) + DMSO (0.28 M) + TEMPO (10 mM). Form I and form II denote supercoiled circular and nicked circular forms, respectively.

As shown in Figure S18 lane 2-3 and Figure 2 lane 2-4, the mobility rate of Form I DNA decreased with the increase of the concentration of $[Ru(bpy)_2(py\text{-}SO_3)]^+$. Meanwhile, the intensity of Form I DNA decreased also with the increase of the concentration of $[Ru(bpy)_2(py\text{-}SO_3)]^+$. Both phenomena may be due to the photoinduced covalent binding of the complex to DNA, which on one hand alters the tertiary structure, apparent molecular weight and net charges of DNA and accordingly the mobility rate, and on the other hand restricts the intercalation of EB and therefore the fluorescence intensity. Thus, from the changes in mobility and intensity of Form I DNA, one may find that DMSO can also reduce the DNA photobinding of the complex, as demonstrated in lane 4 and 6 of Figure S18, presumably due to its competitive coordination to Ru(II) center.

We compared the photo-oxidation products of 9-EtG sensitized by either $[Ru(bpy)_2(py\text{-}SO_3)]^+$ in anaerobic condition or $[Ru(bpy)_3]^{2+}$ in aerobic condition. As shown in Figure S19, signals attributable to M1, M2, M3 and M4 were observed upon irradiating the air-saturated solution of 9-EtG and $[Ru(bpy)_3]^{2+}$. While M3 and M4 originate from the reaction of $^1O_2$ and 9-EtG, M1 and M2 may result from the single electron transfer reaction from 9-EtG to $[Ru(bpy)_3]^{2+}$.[6] In contrast, these products were not observed in the case of $[Ru(bpy)_2(py\text{-}SO_3)]^+$ in anaerobic condition (Figure S8), indicative of different reaction sites or reaction products of DNA and $[Ru(bpy)_2(py\text{-}SO_3)]^+$ with respect to DNA and $[Ru(bpy)_3]^{2+}$.

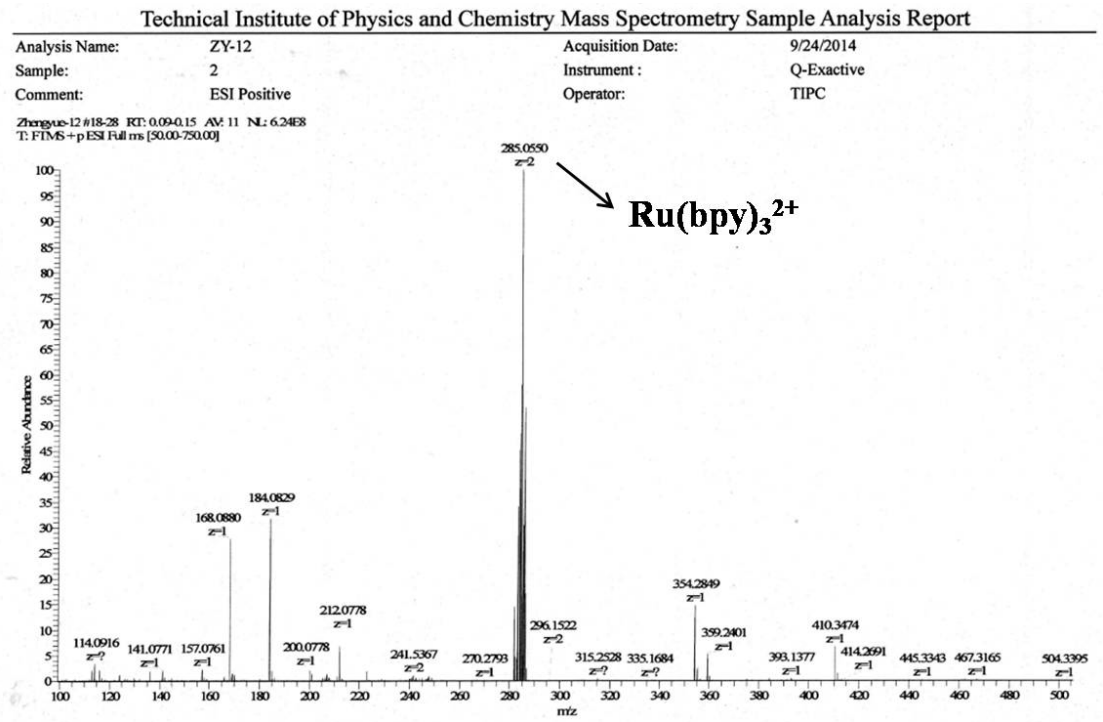

Figure S19. HR ESI-MS spectrum of $[Ru(bpy)_3]^{2+}$ and excess 9-EtG in Air-saturated CH_3COCH_3:H_2O (1.5:1) after irradiation for 1 h.

The oxidation products of 9-EtG are as follows:[6]

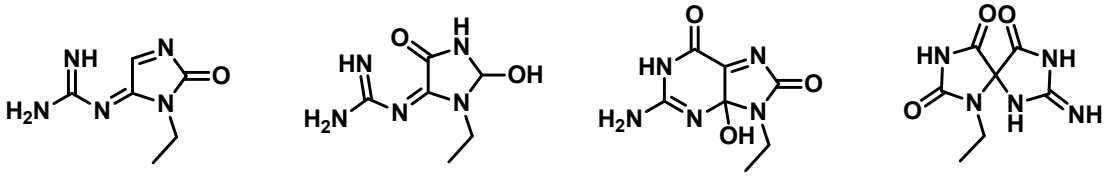

M1 **M2** **M3** **M4**

168.0880 (Calcd m/z for $(M_1+H)^+$ ($C_6H_{10}N_5O$, 168.0885));

184.0829 (Calcd m/z for $(M_2-H)^+$ ($C_6H_{10}N_5O_2$, 184.0834));

212.0778 (Calcd m/z for $(M_3)^+$ ($C_7H_{10}N_5O_3$, 212.0784));

212.0778 (Calcd m/z for $(M_4+H)^+$ ($C_7H_{10}N_5O_3$, 212.0784)).

We further examined the photoreaction products of $[Ru(bpy)_2(py\text{-}SO_3)]^+$ and CT-DNA. Briefly, an Ar-saturated solution (5 mL) of $[Ru(bpy)_2(py\text{-}SO_3)]^+$ (250 μM) and CT-DNA (1 mM) in 5 mM PBS (pH = 7.4) were irradiated for 60 min (≥ 470 nm). The DNA was precipitated with 5 mL of sodium acetate (3.0 M, pH 5.0) and 10 mL of ethanol. Samples were then centrifuged for 30 min at 7000 rpm and decanted. The pellet was rinsed with ethanol (500 μL x 2) and dried under vacuum. 500 μL of HEPES-NaOH buffer (25 mM, pH 8.0) was added and the sample was heated at 90°C for 15 min and quenched in liquid nitrogen. The aqueous solution was then extracted with CH_2Cl_2 and the extract was subjected to EI-MS measurements. As shown in Figure S20, furfural was detected, indicative of H-atom abstract from the C5' position

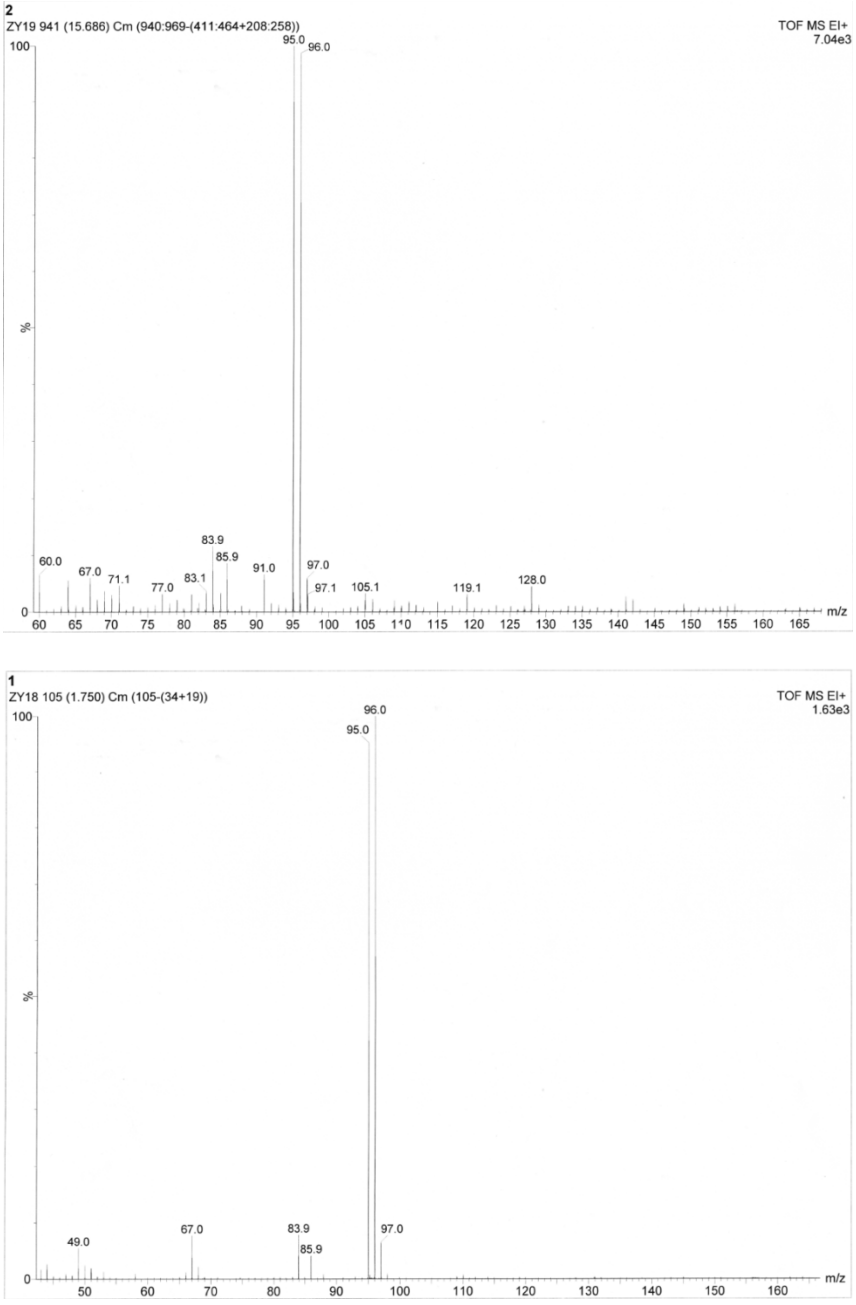

Figure S20. (a) MS spectrum of the CH_2Cl_2 extract from the irradiated sample of $[Ru(bpy)_2(py\text{-}SO_3)]^+$ and CT-DNA. (b) MS spectrum of the CH_2Cl_2 solution of furfural.

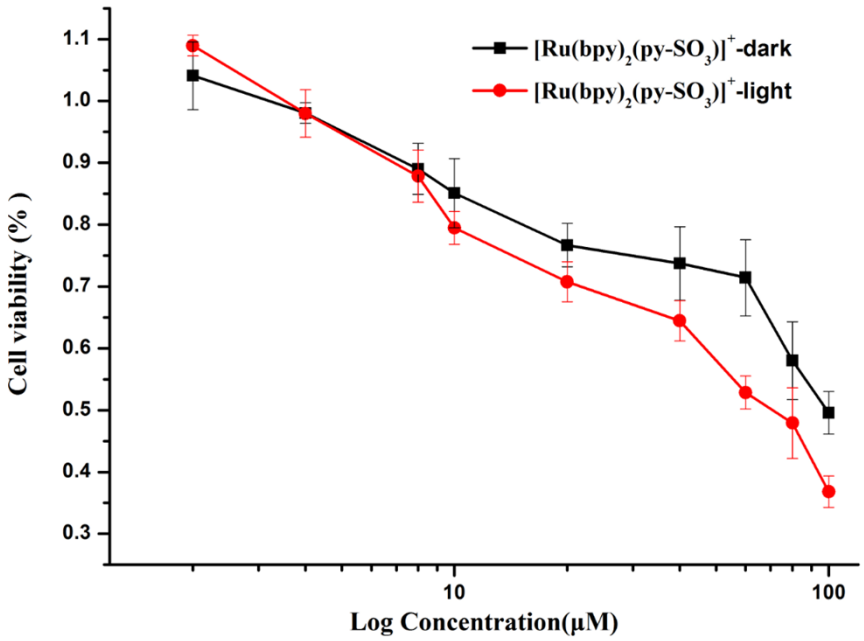

Figure S21. Cytotoxicity dose responses of $[Ru(bpy)_2(py\text{-}SO_3)]^+$ toward A549 cells in the dark (black curve) and upon irradiation for 30 min (≥ 470 nm) (red curve).

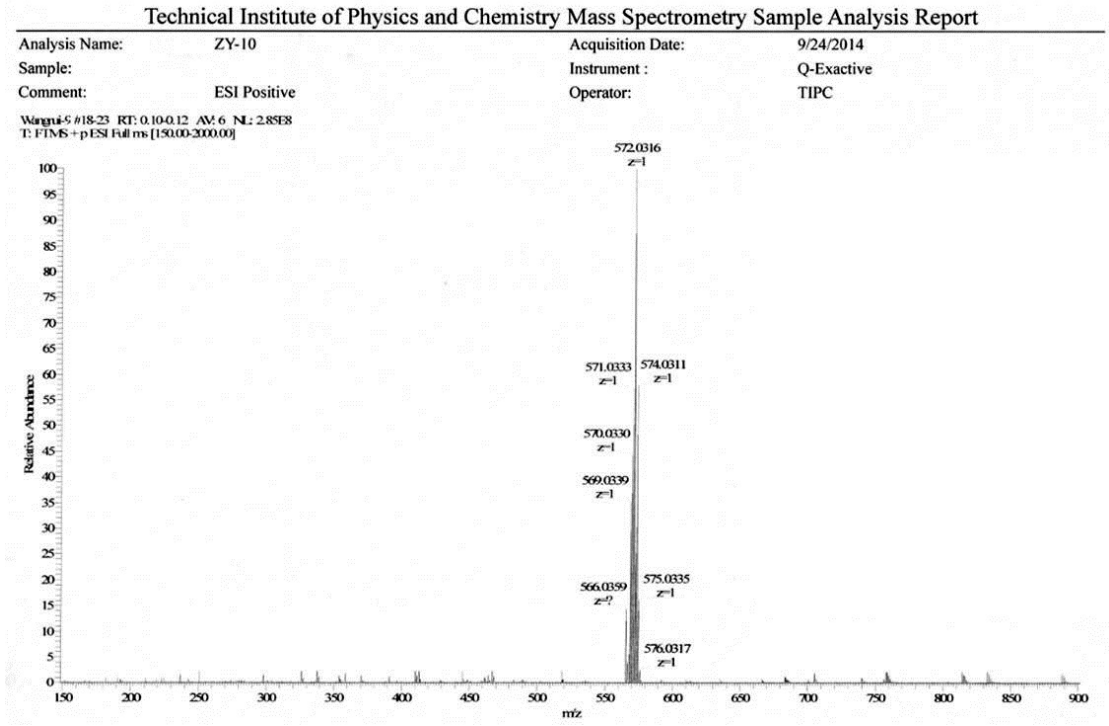

Figure S22. HR ESI-MS spectrum of $[Ru(bpy)_2(py\text{-}SO_3)]^+$ in CH_3CN.

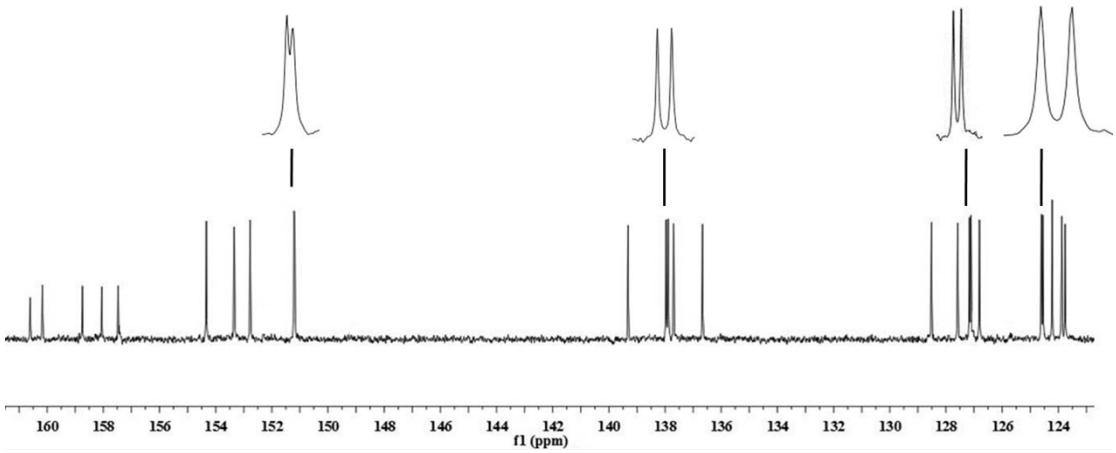

Figure S23. ^{13}C NMR spectrum of $[Ru(bpy)_2(py\text{-}SO_3)]^+$ in CD_3CN.

Table S1. Crystal data and structure refinement for $[Ru(bpy)_2(py\text{-}SO_3)](PF_6)$ (CCDC 1011182).

Empirical formula	$C_{29}H_{26}F_6N_7O_3PRuS$
Formula weight	798.67
Temperature	153(2) K
Wavelength	0.71073 Å
Crystal system, space group	Monoclinic, C2/c
Unit cell dimensions	a = 13.6846(19) Å alpha = 90 deg.
	b = 22.956(3) Å beta = 98.493(2) deg.
	c = 20.732(3) Å gamma = 90 deg.
Volume	6441.4(15) $Å^3$
Z, Calculated density	8, 1.647 Mg/m^3
Absorption coefficient	0.680 mm^{-1}
F(000)	3216
Crystal size	0.40 × 0.25 × 0.25 mm
Theta range for data collection	2.66 to 31.50 deg.
Limiting indices	-19<=h<=20, -32<=k<=33, -29<=l<=30
Reflections collected / unique	31872 / 10684 [R(int) = 0.0348]
Completeness to theta = 31.50	99.5%
Absorption correction	Semi-empirical from equivalents
Max. and min. transmission	0.8484 and 0.7726
Refinement method	Full-matrix least-squares on F^2
Data / restraints / parameters	10684 / 0 / 435
Goodness-of-fit on F^2	0.999
Final R indices [I>2sigma(I)]	R1 = 0.0441, wR2 = 0.1043
R indices (all data)	R1 = 0.0487, wR2 = 0.1082
Extinction coefficient	0.00093(9)
Largest diff. peak and hole	0.777 and -0.950 e.A^-3

Table S2. Bond lengths [Å] and angles [deg] of [Ru(bpy)$_2$(py-SO$_3$)](PF$_6$).

Ru(1)-N(5)	**2.0128(17)**
Ru(1)-N(2)	**2.0476(17)**
Ru(1)-N(4)	**2.0519(17)**
Ru(1)-N(3)	**2.0636(17)**
Ru(1)-N(1)	**2.0796(17)**
Ru(1)-O(1)	**2.1354(15)**
S(1)-O(3)	1.4363(18)
S(1)-O(2)	1.4421(17)
S(1)-O(1)	1.4848(16)
S(1)-C(5)	1.789(2)
N(1)-C(5)	1.346(3)
N(1)-C(1)	1.355(3)
N(2)-C(6)	1.346(3)
N(2)-C(10)	1.364(3)
N(3)-C(15)	1.350(3)
N(3)-C(11)	1.361(3)
N(4)-C(16)	1.352(3)
N(4)-C(20)	1.359(3)
N(5)-C(25)	1.349(3)
N(5)-C(21)	1.361(3)
C(1)-C(2)	1.378(3)
C(1)-H(1)	0.9500
C(2)-C(3)	1.388(3)
C(2)-H(2)	0.9500
C(3)-C(4)	1.387(3)
C(3)-H(3)	0.9500
C(4)-C(5)	1.382(3)
C(4)-H(4)	0.9500
C(6)-C(7)	1.381(3)
C(6)-H(6)	0.9500
C(7)-C(8)	1.388(3)
C(7)-H(7)	0.9500
C(8)-C(9)	1.382(3)
C(8)-H(8)	0.9500
C(9)-C(10)	1.388(3)
C(9)-H(9)	0.9500
C(10)-C(11)	1.471(3)
C(11)-C(12)	1.393(3)
C(12)-C(13)	1.382(3)
C(12)-H(12)	0.9500
C(13)-C(14)	1.383(4)
C(13)-H(13)	0.9500

C(14)-C(15)	1.380(3)
C(14)-H(14)	0.9500
C(15)-H(15)	0.9500
C(16)-C(17)	1.384(3)
C(16)-H(16)	0.9500
C(17)-C(18)	1.385(3)
C(17)-H(17)	0.9500
C(18)-C(19)	1.388(3)
C(18)-H(18)	0.9500
C(19)-C(20)	1.392(3)
C(19)-H(19)	0.9500
C(20)-C(21)	1.471(3)
C(21)-C(22)	1.398(3)
C(22)-C(23)	1.376(3)
C(22)-H(22)	0.9500
C(23)-C(24)	1.387(3)
C(23)-H(23)	0.9500
C(24)-C(25)	1.381(3)
C(24)-H(24)	0.9500
C(25)-H(25)	0.9500
P(1)-F(2)	1.5958(16)
P(1)-F(4)	1.5995(17)
P(1)-F(6)	1.6005(18)
P(1)-F(3)	1.6030(17)
P(1)-F(1)	1.6052(16)
P(1)-F(5)	1.6055(19)
N(6)-C(26)	1.138(5)
C(26)-C(27)	1.432(5)
C(27)-H(27A)	0.9800
C(27)-H(27B)	0.9800
C(27)-H(27C)	0.9800
C(27)-H(27D)	0.9800
C(27)-H(27E)	0.9800
C(27)-H(27R)	0.9800
N(7)-C(28)	1.132(5)
C(28)-C(29)	1.450(5)
C(29)-H(29A)	0.9800
C(29)-H(29B)	0.9800
C(29)-H(29C)	0.9800

N(5)-Ru(1)-N(2)	92.81(7)
N(5)-Ru(1)-N(4)	79.55(7)
N(2)-Ru(1)-N(4)	97.63(7)
N(5)-Ru(1)-N(3)	96.70(7)

N(2)-Ru(1)-N(3)	78.95(7)
N(4)-Ru(1)-N(3)	174.86(7)
N(5)-Ru(1)-N(1)	93.39(7)
N(2)-Ru(1)-N(1)	171.61(7)
N(4)-Ru(1)-N(1)	89.06(7)
N(3)-Ru(1)-N(1)	94.69(7)
N(5)-Ru(1)-O(1)	173.48(7)
N(2)-Ru(1)-O(1)	92.04(6)
N(4)-Ru(1)-O(1)	95.49(7)
N(3)-Ru(1)-O(1)	88.50(7)
N(1)-Ru(1)-O(1)	82.24(6)
O(3)-S(1)-O(2)	114.66(12)
O(3)-S(1)-O(1)	113.21(11)
O(2)-S(1)-O(1)	111.36(10)
O(3)-S(1)-C(5)	106.01(10)
O(2)-S(1)-C(5)	106.64(11)
O(1)-S(1)-C(5)	103.99(9)
S(1)-O(1)-Ru(1)	118.26(9)
C(5)-N(1)-C(1)	116.69(18)
C(5)-N(1)-Ru(1)	117.66(14)
C(1)-N(1)-Ru(1)	125.42(14)
C(6)-N(2)-C(10)	117.99(18)
C(6)-N(2)-Ru(1)	125.95(15)
C(10)-N(2)-Ru(1)	115.98(14)
C(15)-N(3)-C(11)	117.90(18)
C(15)-N(3)-Ru(1)	126.64(15)
C(11)-N(3)-Ru(1)	115.45(14)
C(16)-N(4)-C(20)	118.70(18)
C(16)-N(4)-Ru(1)	126.37(14)
C(20)-N(4)-Ru(1)	114.90(14)
C(25)-N(5)-C(21)	118.55(18)
C(25)-N(5)-Ru(1)	125.62(14)
C(21)-N(5)-Ru(1)	115.66(14)
N(1)-C(1)-C(2)	122.9(2)
N(1)-C(1)-H(1)	118.5
C(2)-C(1)-H(1)	118.5
C(1)-C(2)-C(3)	119.2(2)
C(1)-C(2)-H(2)	120.4
C(3)-C(2)-H(2)	120.4
C(4)-C(3)-C(2)	118.8(2)
C(4)-C(3)-H(3)	120.6
C(2)-C(3)-H(3)	120.6
C(5)-C(4)-C(3)	118.2(2)
C(5)-C(4)-H(4)	120.9

C(3)-C(4)-H(4)	120.9
N(1)-C(5)-C(4)	124.1(2)
N(1)-C(5)-S(1)	116.43(15)
C(4)-C(5)-S(1)	119.49(16)
N(2)-C(6)-C(7)	123.1(2)
N(2)-C(6)-H(6)	118.4
C(7)-C(6)-H(6)	118.4
C(6)-C(7)-C(8)	118.6(2)
C(6)-C(7)-H(7)	120.7
C(8)-C(7)-H(7)	120.7
C(9)-C(8)-C(7)	119.2(2)
C(9)-C(8)-H(8)	120.4
C(7)-C(8)-H(8)	120.4
C(8)-C(9)-C(10)	119.4(2)
C(8)-C(9)-H(9)	120.3
C(10)-C(9)-H(9)	120.3
N(2)-C(10)-C(9)	121.6(2)
N(2)-C(10)-C(11)	114.69(18)
C(9)-C(10)-C(11)	123.67(19)
N(3)-C(11)-C(12)	121.5(2)
N(3)-C(11)-C(10)	114.86(18)
C(12)-C(11)-C(10)	123.65(19)
C(13)-C(12)-C(11)	119.7(2)
C(13)-C(12)-H(12)	120.2
C(11)-C(12)-H(12)	120.2
C(12)-C(13)-C(14)	118.8(2)
C(12)-C(13)-H(13)	120.6
C(14)-C(13)-H(13)	120.6
C(15)-C(14)-C(13)	119.2(2)
C(15)-C(14)-H(14)	120.4
C(13)-C(14)-H(14)	120.4
N(3)-C(15)-C(14)	123.0(2)
N(3)-C(15)-H(15)	118.5
C(14)-C(15)-H(15)	118.5
N(4)-C(16)-C(17)	122.1(2)
N(4)-C(16)-H(16)	119.0
C(17)-C(16)-H(16)	119.0
C(16)-C(17)-C(18)	119.4(2)
C(16)-C(17)-H(17)	120.3
C(18)-C(17)-H(17)	120.3
C(17)-C(18)-C(19)	119.0(2)
C(17)-C(18)-H(18)	120.5
C(19)-C(18)-H(18)	120.5
C(18)-C(19)-C(20)	119.2(2)

C(18)-C(19)-H(19)	120.4
C(20)-C(19)-H(19)	120.4
N(4)-C(20)-C(19)	121.6(2)
N(4)-C(20)-C(21)	114.09(18)
C(19)-C(20)-C(21)	124.34(19)
N(5)-C(21)-C(22)	121.1(2)
N(5)-C(21)-C(20)	114.98(17)
C(22)-C(21)-C(20)	123.94(19)
C(23)-C(22)-C(21)	119.5(2)
C(23)-C(22)-H(22)	120.3
C(21)-C(22)-H(22)	120.3
C(22)-C(23)-C(24)	119.5(2)
C(22)-C(23)-H(23)	120.3
C(24)-C(23)-H(23)	120.3
C(25)-C(24)-C(23)	118.7(2)
C(25)-C(24)-H(24)	120.7
C(23)-C(24)-H(24)	120.7
N(5)-C(25)-C(24)	122.7(2)
N(5)-C(25)-H(25)	118.6
C(24)-C(25)-H(25)	118.6
F(2)-P(1)-F(4)	90.22(9)
F(2)-P(1)-F(6)	90.51(10)
F(4)-P(1)-F(6)	90.50(10)
F(2)-P(1)-F(3)	179.24(11)
F(4)-P(1)-F(3)	90.34(9)
F(6)-P(1)-F(3)	90.01(11)
F(2)-P(1)-F(1)	89.71(9)
F(4)-P(1)-F(1)	179.78(12)
F(6)-P(1)-F(1)	89.71(9)
F(3)-P(1)-F(1)	89.73(9)
F(2)-P(1)-F(5)	90.06(10)
F(4)-P(1)-F(5)	90.00(10)
F(6)-P(1)-F(5)	179.24(10)
F(3)-P(1)-F(5)	89.42(10)
F(1)-P(1)-F(5)	89.79(10)
N(6)-C(26)-C(27)	178.5(4)
C(26)-C(27)-H(27A)	109.5
C(26)-C(27)-H(27B)	109.5
H(27A)-C(27)-H(27B)	109.5
C(26)-C(27)-H(27C)	109.5
H(27A)-C(27)-H(27C)	109.5
H(27B)-C(27)-H(27C)	109.5
C(26)-C(27)-H(27D)	109.5
H(27A)-C(27)-H(27D)	141.1

H(27B)-C(27)-H(27D)	56.3
H(27C)-C(27)-H(27D)	56.3
C(26)-C(27)-H(27E)	109.5
H(27A)-C(27)-H(27E)	56.3
H(27B)-C(27)-H(27E)	141.1
H(27C)-C(27)-H(27E)	56.3
H(27D)-C(27)-H(27E)	109.5
C(26)-C(27)-H(27R)	109.5
H(27A)-C(27)-H(27R)	56.3
H(27B)-C(27)-H(27R)	56.3
H(27C)-C(27)-H(27R)	141.1
H(27D)-C(27)-H(27R)	109.5
H(27E)-C(27)-H(27R)	109.5
N(7)-C(28)-C(29)	179.2(4)
C(28)-C(29)-H(29A)	109.5
C(28)-C(29)-H(29B)	109.5
H(29A)-C(29)-H(29B)	109.5
C(28)-C(29)-H(29C)	109.5
H(29A)-C(29)-H(29C)	109.5
H(29B)-C(29)-H(29C)	109.5

References

[1] B. P. Sullivan, D. J. Salmon, T. J. Meyer, *Inorg. Chem*., 1978, **17**, 3334-3341.

[2] B. S. Howerton, D. K. Heidary, E. C. Glazer, *J. Am. Chem. Soc*., 2012, **134**, 8324-8327.

[3] N. Busto, J. Valladolid, M. Martínez-Alonso, H. J. Lozano, F. A. Jalón, B. R. Manzano, A. M. Rodríguez, M. C. Carrión, T. Biver, J. M. Leal, G. Espino, B. García, *Inorg. Chem*., 2013, **52**, 9962-9974.

[4] (a) E. Ben-hurt, A. Carmichael, P. Riesz, I. Rosenthal, *Int. J. Radiat. Biol.,* 1985, **5**, 837-846;(b) M. M. Mossoba, I. Rosenthal, A. J. Carmichael, P. Riesz., *Photochem. Photobiol.,* 1984, **39**, 731-734.

[5] (a) D. R. Kearns, *Chem. Rev.,*1971, **71**, 395−427; (b) P.R. Ogilby, *Chem. Soc. Rev.,* 2010, **39**, 3181−3209. (c) L. L. Hou, X. Y. Zhang, T. C. Pijper, W. R. Browne, B. L. Feringa, *J. Am. Chem. Soc.,* 2014, **136**, 910-913.

[6] J. Cadet, T. Douki, J. L. Ravanat, *Acc. Chem. Res.* 2008, **41**, 1075-1083.